Post-print of: Ryl J., Zieliński A., Burczyk Ł., Bogdanowicz R., Ossowski T., Darowicki K.: Chemical-Assisted Mechanical Lapping of Thin Boron-Doped Diamond Films: A Fast Route Toward High Electrochemical Performance for Sensing Devices. ELECTROCHIMICA ACTA. Vol. 242, (2017), p. 268-279. DOI: 10.1016/j.electacta.2017.05.027

Chemical-Assisted Mechanical Lapping of Thin Boron-Doped Diamond Films: A Fast Route Toward High Electrochemical Performance for Sensing Devices

Jacek Ryl[a] Artur Zielinski[a], Lukasz Burczyk[a], Robert Bogdanowicz[b], Tadeusz Ossowski[c], Kazimierz Darowicki[a]

[a] Department of Electrochemistry, Corrosion and Materials Engineering, Faculty of Chemistry, Gdansk University of Technology, 11/12 Narutowicza St., 80-233 Gdansk, Poland
[b] Department of Metrology and Optoelectronics, Faculty of Electronics, Telecommunications and Informatics, Gdansk University of Technology, 11/12 Narutowicza St., 80-233 Gdansk, Poland
[c] Department of Analytical Chemistry, Faculty of Chemistry, University of Gdansk, 63 Wita Stwosza St., 80-952 Gdansk, Poland

A B S T R A C T

There is an urgent need for an effective and economically viable increase in electrochemical performance of boron-doped diamond (BDD) electrodes that are used in sensing and electrocatalytic applications. Specifically, one must take into consideration the electrode heterogeneity due to nonhomogenous boron-dopant distribution and the removal of sp2 carbon impurities saturating the electrode, without interference in material integrity. In this work, authors describe a detailed study on electrochemical performance and the enhancement of electrochemical active surface area in the BDD electrodes that have been pretreated via chemical-assisted mechanical lapping.

The effect of lapping on both surface chemistry and oxidation processes at the BDD surface was assessed by means of chronovoltammetry, instantaneous impedance monitoring, and X-Ray photoelec-tron spectroscopy. Next, atomic force microscopy and scanning electron microscopy were employed to produce data on spreading resistance and surface geometry, respectively.

While the analyzed interactions are very complex and multi-level, authors suggested that the main observed effect was due to the removal of non-diamond carbon impurities from the electrode surface, decreased grain size, and heterogeneous conductivity. Short-duration pretreatments were found to be an effective route towards more efficient surface activation with negligible alterations in the diamond film structure. A prolonged pretreatment led to a decrease in grain size and lowered contribution of (111) and (110) facets, which in turn influenced the electrode kinetics.

Keywords: boron doped diamond, electrode homogeneity, spreading resistance, impedance monitoring

1. Introduction

Recently, the electrochemical applications of boron-doped diamond (BDD) electrodes attract much attention not only in the field of electrochemistry, but also in other areas such as functional materials, analytical and environmental chemistry, biomedical and biological sciences. Since the properties of BDD are combined with its inert surface characteristics, the BDD electrodes display intriguing electrochemical features, *inter alia*, the widest solvent window of all electrode materials in aqueous solutions, low background and capacitive currents, reduced fouling and the ability to withstand extreme potentials, while at the same time retaining the excellent mechanical robustness. Thus, BDD is slowly rising in prominence in the electrochemical arena, predominantly where longevity and low maintenance are key attributes [1,2].

The electrode preparation step is often applied to remove sp^2-carbon impurities saturating the BDD electrode during the CVD process [3,4], which can be found in particular, but are not limited to, inter-grain regions [5]. Usually, the pretreatment of BDD electrode surface for electrochemical measurements is carried out via one or several of the following mechanisms: (I) mechanical polishing and lapping; (II) acid washing and rehydrogenation; (III) heat treatment; and (IV) electrochemical polarization [6–11] (Supporting Information, Section I). These methods are often

http://dx.doi.org/10.1016/j.electacta.2017.05.027

found to be destructive as they introduce stresses to the BDD film, which may lead to the formation of cracks and film discontinuities. The destructive nature of the pretreatment process depends on many factors, such as growth method, film thickness and the presence of sp^2-carbon phase.

The numerous types of chemical and mechanical pretreatments are characterized by distinctive disadvantages [12–16]. The final surface finish and the level of interference into the material's physico-chemical properties greatly depends on the chosen pretreatment method. This, in turn, affects the factors such as grain size or oxidation of termination bonds [17], both being of key interest to electrochemical performance of BDD electrodes. The termination bonds not only substantially influence the electrochemical properties of diamond [18,19] but also factors such as hydrophilicity or adhesion and durability of organic compounds attached to the electrode surface [20,21]. For example, Bogdanowicz et al. [22] reported that the difference in anodic polarization of even 0.2 V may lead to an almost complete detachment of functionalized amine film from the electrode surface.

The numerous indirect analytical approaches have demonstrated the occurrence of heterogeneity of physico-chemical properties within grain boundaries in polycrystalline BDD films [23,24]; the resulting effect can be critical in cases when high performance is expected in electrochemical applications. It is assumed that polycrystalline boron-doped diamond surfaces exhibit heterogeneity in electron-transfer rates over the surface due to non-uniform distribution of dopant throughout the film, with local highly-doped sites of fast (reversible) kinetics and the slow sites (irreversible) containing less dopant [25–27]. Recently, nanoscale impedance microscopy (NIM) allowed the observation of differences in impedance modulus between the areas of different boron-dopant concentration, which amounted to three orders of magnitude between the grain boundaries and inter-grain regions [5]. This phenomenon originates from the higher boron incorporation at the grain boundaries, which results in the much lower charge transfer resistance. In addition, the preferential sp^2-carbon contamination in the inter-grain regions plays a significant role. Based on the above mentioned results, it has been assumed that the electrochemically active surface area is much smaller than the geometrical surface area. As a consequence, large heterogeneities of electric properties should be expected for high local current densities at conductive regions [28,29], leading to the lowered electrode efficiency and accelerated electrode aging. The effective reaction rate constant strongly depends on the coverage of inactive area. Furthermore, the heterogeneity of physico-chemical properties occurs at the level of particular grains. Szunerits et al. [30] claim that the dopant level in particular grains varies which can result in the two types of region, with different metallic and semiconducting properties next to each other.

To the best of our knowledge, there has been no earlier contribution to the discussion on the effect of chemical-assisted mechanical lapping (CAML) on electrochemical properties of BDD electrodes. The authors have proposed this particular pretreatment technique as a possible route to increase the electrode's performance in a fast and effective way, taking into consideration that the removal of *sp*- and sp^2-hybridized carbon is much faster than the removal of stable sp^3 phase, while lapping itself does not strongly affect the material integrity [31,32]. The CAML effect has been studied with AC and DC electrochemical techniques as well as various microscopic and spectroscopic tools. The presented work demonstrates the changes in electrochemical properties of as-prepared Si/BDD electrodes, while the applied pretreatment technique is shown to be even more efficient in the case of electrodes that have become degraded due electrochemical fouling.

2. Experimental

The boron-doped diamond was synthesized in an MWPECVD system (SEKI Technotron AX5400S, Japan) on p-type Si substrates with (111) orientation. The seeding process included spinning of thin film of DND seeding media by means of a spin-coater (Laurell WS-400B, USA). The home-made DMSO-PVA-DND suspension with nanodiamond concentration of 0.25% w/w in DMSO/PVA was used in the experiments. The procedure for DND slurry preparation has been reported elsewhere [33]. The selected substrates were etched in hydrogen plasma for 1 min. The optimized power of microwave plasma for diamond synthesis was kept at 1300 W. Excited plasma was ignited by microwave radiation (2.45 GHz). The total flow of gas mixture, containing 1% of the molar ratio of CH_4–H_2, was kept at 300 sccm. Diborane (B_2H_6) was used as dopant precursor, and the [B]/[C] ratio of boron level in the gas phase was kept at 10 000 ppm. The used growth time of 6 h produced microcrystalline hydrogen-terminated diamond films of ca. 2 μm in thickness.

The Si/BDD electrodes underwent chemical-assisted mechanical lapping on an own-designed lapping machine. Samples had surface area of 1 cm^2. The rotational speed of pad and carrier (rotating in opposite directions) equaled to 40 rpm, while the down pressure was 40 kPa. Samples were attached to the carrier with silver paste and subjected to CAML for different time periods (t), i.e. 3, 10, 30, 80 and 120 min. The cloth was moistened at a rate of 100 ml h^{-1} with an alkaline colloidal silica solution. The size of silica particles (Akasel, Denmark) was 50 nm in diameter. Buehler 40-7212 PSA polymer microcloth was used. Immediately after the CAML pretreatment, samples were degreased in acetone with an ultrasonic cleaner.

Selection of lapping parameters was based on a procedure carried out for nanocrystalline diamond [34,35] and it might require further optimization for different types of diamond-based electrodes. According to Thomas et al. [34] this inexpensive and efficient method is based on the chemical-assisted mechanism, consisting of wet oxidation of the surfaces with the polishing fluid, followed by the formation of $Si(OH)_4$ passive layer and eventually shearing silanol molecules with bonded carbon atoms from the electrode surface. It is concluded that the lapping does not significantly change the chemical composition of NCD surface, and thus the graphite and graphite-related defects were not developed.

The chronovoltammetric and impedance measurements were performed by means of an Autolab 302N potentiostat/galvanostat (Ecochemie, The Netherlands). In the case of impedance measurements, the system was expanded with PXIe-4464 and PXIe-6124 (National Instruments, USA) measurement cards for AC signal generation and acquisition, respectively. The aforementioned cards were operating in PXIe-1073 chassis. The measurements were carried out in a three-electrode cell, with Si/BDD as a working electrode, $Ag|Ag_2SO_4$ as a reference electrode (+0.273 V vs SHE), and the platinum mesh as a counter electrode. The sample area submitted to electrochemical investigations was 0.50 cm^2; it was limited by the geometry of electrochemical cell. The volume of electrochemical cell was 50 ml. The $Ag|Ag_2SO_4$ reference electrode was prepared in accordance with the methodology presented elsewhere [36,37] in order to avoid chloride contamination. Chronovoltammetry served as a tool to define changes in the active surface area due to lapping. The scan rate was set between 5 and 100 mV s^{-1}, while the polarization ranged from −0.6 to +1.2 V vs $Ag|Ag_2SO_4$. A solution of 5 mM $K_4[Fe(CN)_6]$ + 0.5 M Na_2SO_4 was used as an electrolyte. Ferri/ferrocyanide remains the most often used redox couple to investigate BDD electrodes, although a number of sources fairly report its lack of reproducibility if electrodes have different electrochemical history [38–40]. To avoid it, a new electrode was used for each subsequent measurement.

Contact mode atomic force microscopy (AFM) and scanning electron microscopy (SEM) were employed to characterize the surface topography of BDD film. The SEM analysis was carried out by means of S-3400N microscope (Hitachi, Japan) with a tungsten light source. The secondary electron detector was used, which operated under the accelerating voltage of 20 kV. The SEM images of BDD surface were quantified using the program for data visualization and analysis (Gwyddion, 2.40, Czech Republic) [41]. The AFM measurements were carried out using NTEGRA Prima microscope (NT-MDT, Russia) with CTD-NCHR conductive probes (Nanosensors, Switzerland). The parameters of the probes were as follows: cantilever length (L) of 115–135 μm, force constant (k) of 23–225 N m^{-1}, and the resonance frequency (f) of 225–610 Hz. Based on the parameters of individual probes, the force of contact was estimated to be 1.2 μN. The spreading resistance was determined by measuring the current flowing through the sample-tip contact due to the application of a constant bias voltage equal to 50 mV. The quality and the type of probes used in measurements are crucial for AFM measurements with simultaneous electrical characterization [42]. Initial validation revealed best performance of diamond coated probes due to their resistance to mechanical wear and relatively high conductivity [43]. The additional information related to the probe selection for the spreading resistance mapping is presented in Supporting Information, Section II.

The influence of CAML pretreatment on the surface chemistry of analyzed specimens was studied by using X-Ray Photoelectron Spectroscopy (XPS) with Escalab 250 Xi (ThermoFisher Scientific, United Kingdom). The aforementioned device employs Al K□ monochromatic light source, with a spot diameter of 650 μm. The high-resolution spectra were recorded for C1s and O1s regions at the energy step of 0.1 eV and a pass energy of 10 eV. In order to normalize the obtained spectroscopic measurements, the X axis (binding energy, BE) of XPS spectrum was calibrated in reference to the peak characteristics of neutral C1 s (BE = 284.6 eV). The peak deconvolution was performed by using Avantage software provided by the manufacturer.

Irrespective of other conducted testing, the CAML pretreated electrodes were subjected to Dynamic Electrochemical Impedance Spectroscopy (DEIS) in potentiodynamic mode for the polarization range from −1.5 to +2.5 V vs $Ag|Ag_2SO_4$ to verify the influence of chemical-assisted mechanical lapping on the mechanism of surface termination under anodic oxidation. The DEIS characterization was performed in 1 M H_2SO_4 (electrolyte) without any additional preparations. The goal was to compare the obtained DEIS results with those reported by the author in previous studies [36,44]. The measurements were carried out for the frequency range between 94 kHz and 7 Hz, and the sampling frequency of 204.8 kHz. A multisine perturbation signal was composed of 29 sinusoids with 8 points per decade. The peak-to-peak amplitude of perturbation signal did not exceed 30 mV. The resulting signal was sequenced with an analyzing window of 1 s in length, and subjected to Short-Time Discrete Fourier Transformation. DC scan rate during DEIS measurement was 1 mV/s, keeping system in quasi-stationary conditions in the applied analyzing window throughout the measurement. A detailed description of DEIS analysis was presented elsewhere [45,46].

3. Results and discussion

Initially, the influence of CAML on the Si/BDD topography, roughness and grain size was investigated by means of AFM. The topography imaging was carried out in order to estimate the geometric surface area. It was demonstrated that CAML causes an apparent change in the geometric structure and surface roughness of the analyzed samples. The average roughness (S_a), which was used to quantitatively assess the surface roughness, is defined in accordance with ISO 25178-2 as in Eq. (1):

$$S_a = \frac{1}{MN}\sum_{k=0}^{M-1}\sum_{l=0}^{N-1}|z(k.l)| \quad (1)$$

where M and N are dimensions of the scanned area (256 pixels each in this study), and z(k,l) is the height of each pixel indexed by the k and l coordinates.

Fig. 1 shows changes in sample roughness as a function of CAML duration. The zero point corresponds to the reference sample which has not been subjected to the process. The initial decline in S_a is noticeable, which can be explained by the mechanical leveling of height differences. For longer time periods (>100 min), this decline is negligible.

However, in the case of heterogeneous samples, the estimate of their actual surface geometry cannot be easily translated into the electrochemically-active surface area. Several literature reports [47,48] demonstrated that there are differences in the values of electric parameters measured in different areas on the surface of BDD electrode. For example, high discrepancies in the charge

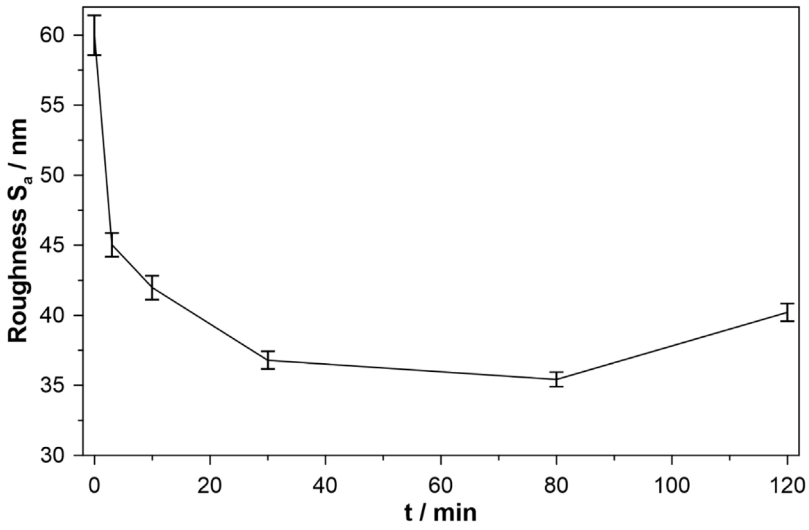

Fig. 1. Change of surface roughness S_a, as a result of CAML, obtained on the base of AFM measurements.

transfer resistance were found that significantly reduce the real reaction plane of the electrode.

In order to estimate the spatial distribution of regions characterized by different conductivity, the spreading resistance mapping was performed in parallel with topography imaging. In the past, the application of mapping technique revealed the effect of differences in conductivity on the efficiency of produced electronic components [49] and the degree of corrosion attack [50], where defining a relationship between the microscopic surface structure, distribution of electrical field, and macroscopic performance was of high importance [51]. A similar approach has also been applied to elucidate the spatially-heterogeneous electrical properties of hydrogen-terminated BDD electrodes [25,52,53]. Thus, the distribution of spreading resistance may constitute the important characteristic of heterogeneous materials.

The results of spreading resistance mapping are depicted in Fig. 2d-f. The significant spatial heterogeneity of the electrodes was observed, with the variation of local conductivity of up to 3 orders of magnitude. The measurements confirmed the non-uniform distribution of conductivity among the data sets of the analyzed surface areas of Si/BDD film [5,52,53]. A noticeable decrease in spreading resistance was observed at the crystallite boundaries compared to the inter-grain regions, which is most likely related to the difference in boron doping density.

Generally, in the case of BDD films there are many parameters besides boron concentration that influence charge transport thus conductivity like grain size distribution, specific structures of B defects or the amount of conductive carbon [54–56]. However, most of previous studies shows that varied boron concentration influences above mentioned microscopic parameters. Thus, it provides higher conductivity modifying it directly or in-directly [57]. With increasing boron concentration, a spread in the energy of the localized states of boron impurity centers induces the formation of an impurity band (with a band width of ~0.2 eV for a boron concentration of $\sim 10^{19}\,cm^{-3}$) and hopping conduction through nearest-neighbors or more distant impurities takes place [58]. Furthermore, other techniques like imaging STEM probe acquiring an EELS spectrum, clearly shows an enrichment of boron at the intergrain regions of 1-2 orders of magnitude, while it stays relatively stable [59] at the diamond grains. That result support normalized spreading resistance maps illustrated in Fig. 2.

On the other hand, defects caused by boron diffusion could also be responsible for the observed conductivity variation. The hydrogen atoms diffuse in the boron-doped diamond at a relatively fast rate because they migrate as protons, with a low migration energy (0.1–0.2 eV). Such protons are trapped by boron acceptors which results in the formation of (B,H) complexes and the passivation of boron acceptors by hydrogen [60]. The resulting diamond films usually show in the Raman or FTIR hydrogen-related local vibrational modes due to the presence of $C—CH_x$ at the intergrain regions [61,62]. This effect is depth-limited and can be eliminated by CAML pretreatment.

The binarization of images was performed to compare the conductivity of samples for varying CAML durations, and different pretreatment methods. Authors proposed to include an additional parameter (i.e. the fraction of active surface χ) in order to define the surface area fraction at the nanoscale, which would be expressed by the value of spreading resistance not higher than the chosen threshold. The goal of this procedure was to estimate the

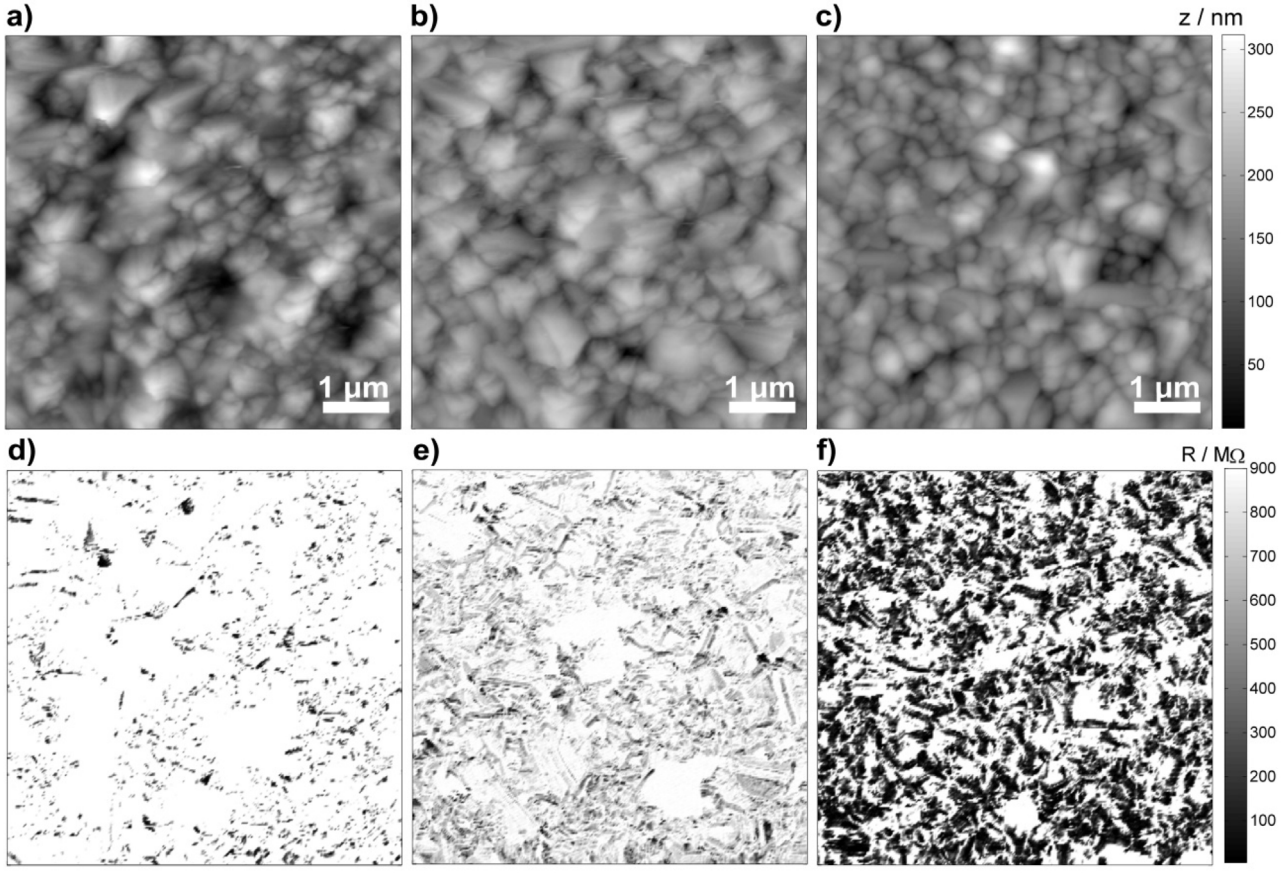

Fig. 2. AFM topography maps for a) the reference sample, b) after 10 min of lapping, and c) after 120 min of lapping; d-f) normalized spreading resistance maps of the respective regions, revealing heterogeneity of electric properties of Si/BDD electrodes.

effect of non-uniform distribution of electrochemically-active surface area, which depends on the assumption that the surface area possessing the lowest resistance dominates the charge transfer processes at the interface. The aforementioned assumption is particularly appropriate in the case of processes limited by high diffusion resistance or carried out over the short time scale, which result in the apparent heterogeneity of rate constants [25]. Thresholds between 5 and 90% of the maximum recorded spreading resistance were chosen, while the maximum registered spreading resistance was close to 900 MΩ for each sample. The results of the above-mentioned procedure are shown in Fig. 3.

It can be deduced that the duration of CAML pretreatment results in the higher fraction of active surface χ regardless of the assumed threshold value. This relationship was only distorted for the longest CAML duration of 120 min, which most likely occurred due to the damage made to the electrode (a detailed discussion is presented further). The fraction of highly conductive electrode area increases with increasing boron-doping level, while still showing high spatial heterogeneity [52,63,64]. The different degree of heterogeneity is connected to inhomogeneous boron doping as well as the variable work function or variable hydrogen content.

In general, the ability to prepare low-resistivity diamond thin films stimulated the present research effort to characterize the electrochemical activity of this material [65]. Local lowering of the films resistivity gives rise to the relatively more 'ideal' voltammetric responses recorded at diamond thin-films. Next, the variation of the voltammetric waveshape as a function of the analyte concentration and as a function of the scan rate strongly indicates that the electrodes themselves are significantly resistive leading to the distorted voltammetric waveshape and subsequent suppression of the peak heights, as compared to the Randles-Sevcík equation at high scan rates and high analyte concentrations [66]. Furthermore, the electrochemical formation of charge carriers in the diamond particles, percolation theory, and charge screening at the double layer, charge transport on diamond particles depends not only on the intrinsic surface conductivity of individual diamond particles but also particle-to-particle charge transfer [67].

In order to verify AFM results on the electrochemical behavior and the active surface area at the macroscale, cyclic voltammetry was performed with presence of $Fe(CN)_6^{4-}/^{3-}$. Fig. 4a and b show the normalized CV curves whose shape is changing as a result of different scan rates. Based on the distance between the anodic and cathodic peaks, it is apparent that the process is quasi-reversible (see Table 1). Such scenario can be expected for the electrodes characterized by the spatial heterogeneity of electric properties [2,25,52,63]. The following relationship can be expressed with the modified Randles-Sevcik formula (2) [68]:

$$i_{p,a} = 3.0 * 10^5 n\alpha^{3/2} A v^{1/2} {D_{red}}^{1/2} c \quad (2)$$

where $i_{p,a}$ is the anodic peak current in amps, v is the polarization sweep rate in V s^{-1}, n is the number of electrons transferred during the redox reaction, D_{red} is the diffusion coefficient of $Fe(CN)_6^{4-}$, C is a concentration in mol cm^{-3}, and $\alpha = 0.5$ is a transfer coefficient. The value of theoretical diffusion coefficient equal to 6.67×10^{-6} $cm^2\ s^{-1}$ was taken from literature data [69]. Due to the fact that diffusion process undergoes on partially blocked electrodes deviations in Eq. (2) are expected [70], and the obtained surfaces' area can be treated as relative ones, used to relate them with AFM data.

A linear ratio between $i_{p,a}$ and $v^{1/2}$ was estimated (see Fig. 4c) which allowed the determination of active surface area, A. The variation of active surface area, estimated from Eq. (2), is presented in Fig. 4d. It is apparent that initially the slope becomes steeper over time. However, after the initial 10 min, it starts to decrease. The applied CAML process led to a decrease in the geometric surface area starting in the first minute of treatment, as observed in the AFM study. In the case of short CAML durations, the opposite effect was observed for the active area. The values of linear correlation coefficient and slope for each investigated sample are presented in Table 1.

The AFM and CV results allowed the evaluation of CAML effect on the development of electrode active area. AFM measurements allows for direct determination of conductive regions. On the other hand, determination of active surface in electrochemical approach is based on determination of overall currents, affected by electrode heterogeneity. This problem was a topic of several theoretical evaluations [22,71–74]. Parameters related to the blocking surface and the lateral diffusion in the non-homogeneous transport layer should be taken into consideration to obtain comparable data. Both approaches confirmed a significant change in electric properties of Si/BDD electrodes. The visible trends of changes detected via

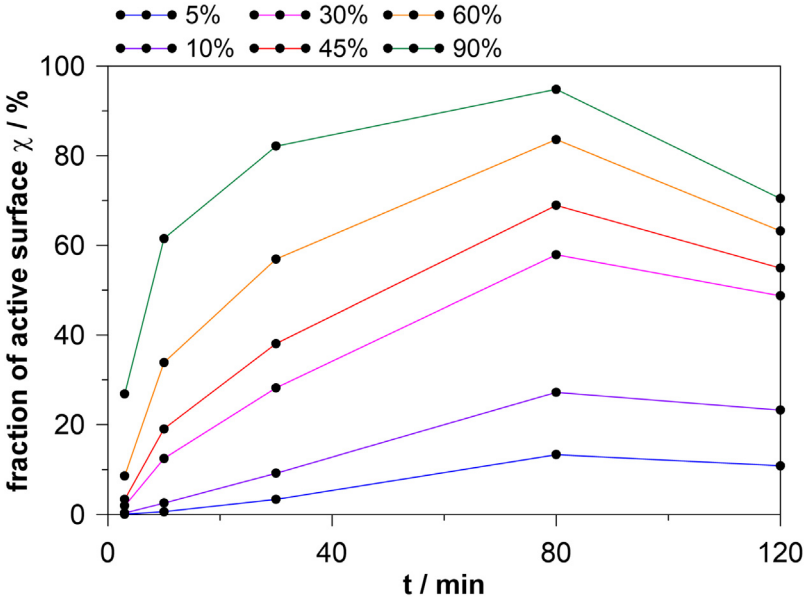

Fig. 3. Estimation of impact of CAML on fraction of active surface χ on the base of different thresholds of the maximum recorded values of the local electric resistance.

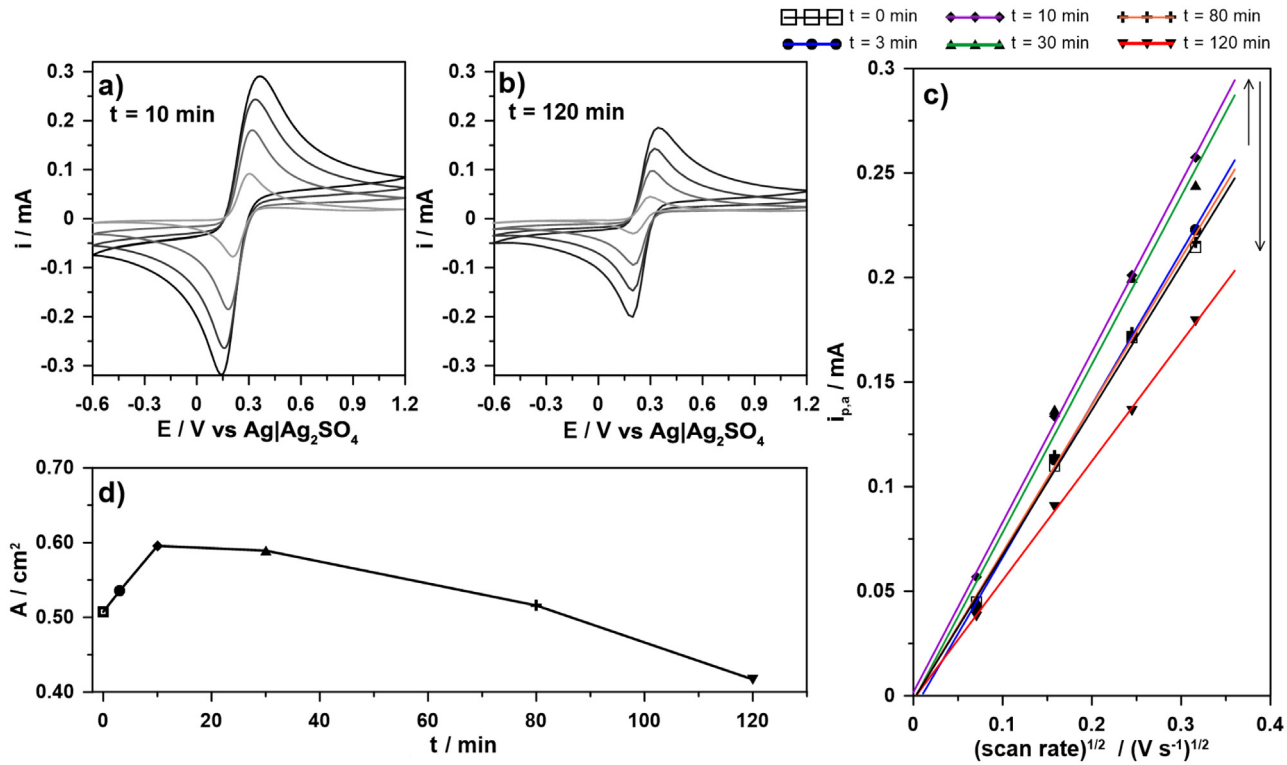

Fig. 4. Chronovoltammograms for CAML duration of a) 10 min, b) 120 min, obtained for $Fe(CN)_6^{4-/3-}$ oxidation/reduction process; c) the slope of $i_{p,a} = f(v^{1/2})$ function; d) the change of active surface area on the base of eq. (2), $\alpha = 0.5$.

electrochemical approach and spreading resistance mapping approach appear to be in agreement. The diversification was primarily observed for long CAML treatments. Moreover, the observed changes correlate to variation of surface roughness (Fig. 1). While the local trends of spatial heterogeneity of conductivity persist, the CAML effect is more general in nature and it is most likely connected to the interference in material structure and/or removal of surface contaminations grown during CVD process [75]. On the other hand, the change of termination type should not be considered to cause this effect because OT-BDD possesses higher surface resistance than HT-BDD [6,76].

Studies on the depth incorporation of boron in the BDD electrodes, carried out by means of elastic recoil detection and secondary ion mass spectroscopy, have led to the conclusion about its uniform distribution among the highly boron-doped film, regardless of doping level [77,78]. Simultaneously, a gradual decrease in hydrogen concentration along the depth profile was observed. Hydrogen affects the electrochemical performance and increases conductivity through the increased hole conduction [79]. On the other hand, it can reduce the conductivity of boron-doped diamond by forming acceptor-donor complexes with substitutionally-inserted boron [60].

Table 1
The potential difference between oxidation and reduction peaks registered at scan rate of 5 mV/s and slope for Randles-Sevcik formula along with correlation coefficient R^2 obtained for each investigated sample.

t/min	$\Delta E_{5mV/s}$/mV	$(i_{p,a}/v^{1/2})$ slope	R^2
0	98	0.6927	0.999
5	102	0.7306	0.999
10	95	0.8130	1.000
30	104	0.8044	0.993
80	97	0.7042	0.998
120	137	0.5691	1.000

In order to reveal possible changes in the Si/BDD microstructure, the scanning electron microscope (SEM) studies were performed. The SEM micrographs presented in Fig. 5 reveal the flattening of BDD surface and a decrease in the crystallite size. The size and distribution of crystallites was statistically averaged over the area of 12×8 μm, with a 0.5 μm interval, on the scale from 0.5 to 2 μm. The relative surface area coverage was obtained by multiplying the number of crystallites by their surface area. A similar approach was previously reported by Bogdanowicz et al. [80].

The surface of reference sample was mostly covered by crystallites with the mean grain size ranging between 1 and 2 μm. As Si/BDD electrodes are lapped, the number of crystallites larger than 2 μm drops down to zero, while the mean grain size decreases by 0.5 μm. Eventually, 34 and 72% of surface area becomes covered with grains not larger than ca. 0.5 and 1.0 μm in size, respectively. The presented observation is supported by the fact that under fixed growth conditions, the size of crystalline facets increases with increasing film thickness. Therefore, the lapping of BDD film may result in decreased grain size [81]. The Si/BDD electrodes are characterized by higher electric conductivity at the grain boundaries due to a difference in boron incorporation. The application of CAML pretreatment results in the higher fraction of inter-grain regions, which validates the influence of microstructure on the electric properties of Si/BDD electrode at the macroscale.

The thinning of BDD layer might not be a sufficient explanation, while an increase in the surface conductivity appears to be of a more complex nature. As-grown BDD samples mostly consist of relatively large (111) and (110) faceted crystals as demonstrated in this work by SEM, or by XRD which had been reported earlier by Wang et al. [82]. The aforementioned planes have been visualized in Fig. 5a–c with a light green color. It was observed that the number of grains of specific crystallographic orientation gradually decreases with increasing CAML duration. The SEM image analysis

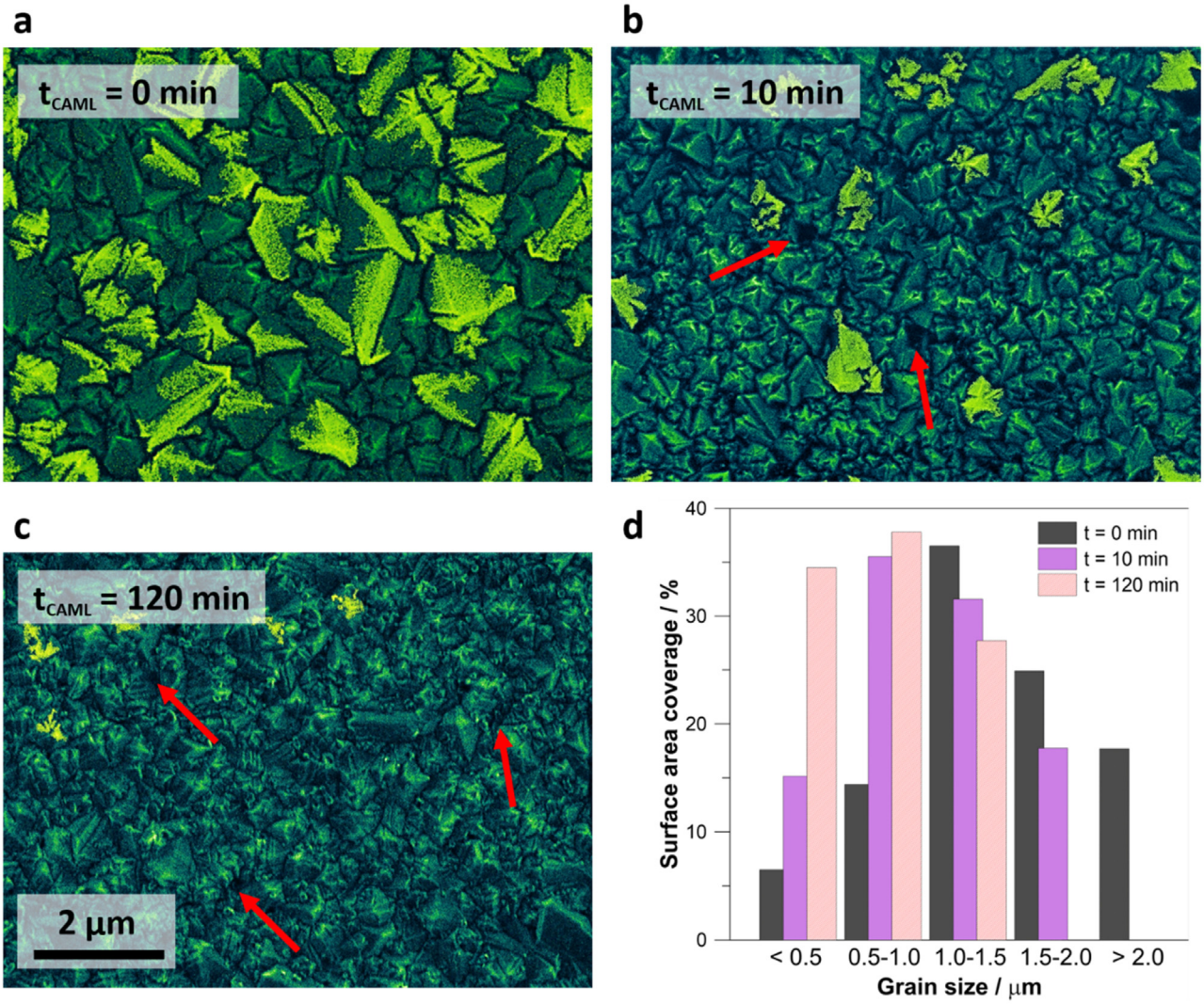

Fig. 5. SEM micro-images of boron-doped polycrystalline diamond surface after CAML: a) as-grown reference, b) 10 min, c) 120 min; d) Plot of grain size distribution of BDD surface vs duration of CAML. Surface grain analysis was performed using Otsu's method of grain detection and filtering implemented in Gwyddion program.

showed that the planes have been scratched first (long cracks along (111) in Fig. 5b) and eventually removed, creating a rough disordered surface (Fig. 5c).

Although the underlying mechanism is not well understood, the existence of "soft" and "hard" grinding directions during polishing or lapping is a recognized phenomenon that greatly affects the diamond removal rates and depends on the properties of electrode material because there may be only a few preferential grinding directions for each face [83,84]. As a result, in "soft" directions the surface possesses an optical finish, while the "hard" direction leaves a rougher surface. The "soft"/"hard" removal rate depends on the process conditions and vary between different studies, yet it seems to be much higher for (100)-oriented crystals, making them harder to wear down homogeneously [85]. Since boron incorporation differs between the grains of different crystallographic orientation [64,86,87], the subsequent selective removal of (111) and (110)-oriented crystals will to some extent correspond to macroscopic electrochemical performance, lowering the electrochemically active surface area in the case of prolonged CAML pretreatments.

The anisotropic wear in the aforementioned films was previously reported by El-Dasher et al. [88]. The occurrence of pits resulting from the mechanical force pulling out the surface grains was also demonstrated [17,84]. The pits visible on the SEM images were present at the grain boundaries in samples treated with prolonged CAML. The presence of cavities and microchipping in crystallites corresponds to a slight increase in geometric area (see Fig. 1) and a decrease in the electrochemically-active surface area reported earlier (see Figs. 3 and 4). Therefore, short-time lapping procedure is typically applied [81,89].

Nevertheless, no cracks or discontinuities were found in the analyzed BDD films, which means that Si substrate did not interfere into the electrochemical system. This finding constitutes a great advantage over other, more invasive pretreatment methods. A comparison between CAML and the most commonly used pretreatment method (acid washing/plasma hydrogenation) with respect to the electrochemical active surface area is presented in Supporting information, Section III and IV.

The X-Ray Photoelectron Spectroscopy analysis was carried out in order to determine the changes in surface chemistry of Si/BDD electrodes after CAML pretreatment. These studies were performed for the energy range of C1s, O1s and Si2p3. High resolution spectra for carbon 1s, as presented in Fig. 6, were deconvoluted into five components that had been successfully used in previous studies of Si/BDD electrodes with a similar doping level [36,90–93]. There are two dominant components in the case of the reference

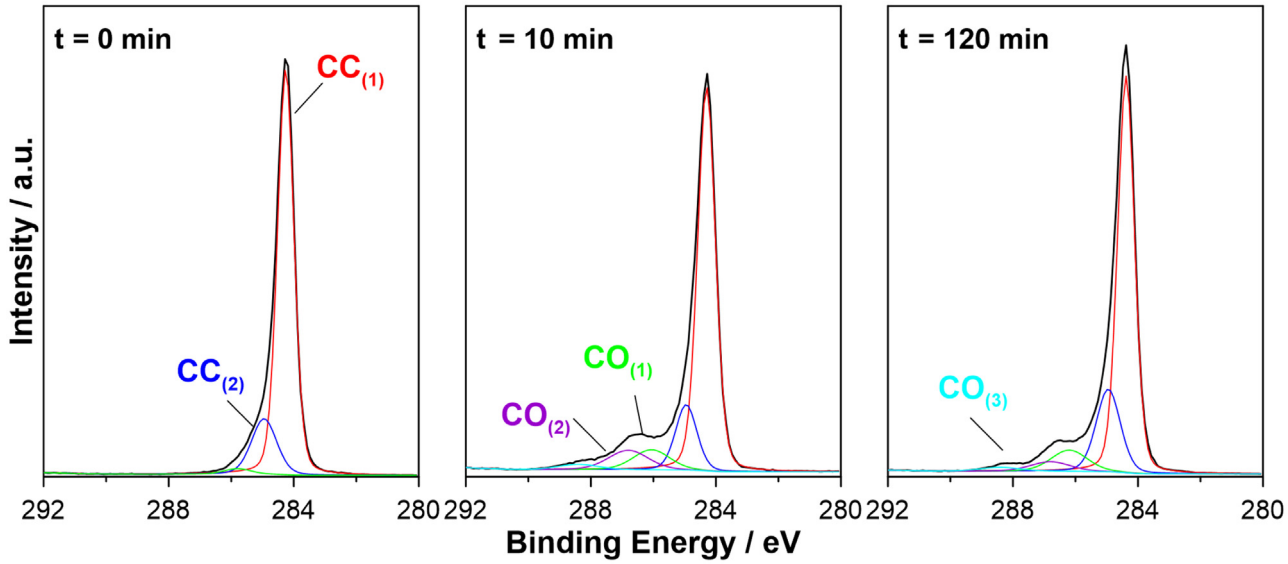

Fig. 6. High resolution XPS spectra recorded in the energy range of C1 s for BDD reference electrode and after different times of CAML process.

sample, i.e. $CC_{(1)}$ at 284.4 eV, and $CC_{(2)}$ at 285.0 eV. The first of these two peaks can be attributed to the C-H bonds on the surface and the C-C bonds in bulk diamond, while the second peak corresponds to the non-hydrogenated BDD surface and polyhydride carbon species (CHx) adsorbed on the surface [94]. As a result of CAML, the chemistry of the BDD electrode surface has changed. A wide tail visible in the C1s spectra of lapped samples was deconvoluted into three additional peaks, namely, $CO_{(1)}$, $CO_{(2)}$ and $CO_{(3)}$. These peaks are shifted from +1.4 eV up to +4.1 eV relative to the $CC_{(1)}$ peak, which should be attributed to the appearance of ether, carboxyl and carbonyl groups.

Considering our findings, it should be noted that CAML pretreatment affects the termination of Si/BDD electrode in a similar way, regardless of the process duration. With respect to the reference sample, a much higher contribution of C-O bonds was observed. Overall, after only three minutes of CAML process the CC/CO ratio dropped five times, although it remained at the same level throughout the rest of the experiment. As previously observed by Thomas et al. [34] for nanocrystalline diamond films, CAML might contaminate the processed surface via the polishing pad and slurry (see Supporting information, Section V). Initially, silicon is not observed in the reference sample. It appears as a result of the lapping process, with a peak doublet (Si2p3 at 103.6 eV) at the energy range of SiO_2. The amount of silicon does not increase over time, and the O/Si ratio remains almost the same, which proves that the BDD film has not been stripped off or extensively thinned. The oxygen content reached up to 15 at.% in total, the amount which is often observed in the case of exposure to atmospheric conditions. Contrary to deep anodic oxidation, sp^2-type defects, manifested as peaks shifted by about −1 eV from the main diamond C1s component, were not found at the diamond interface. Small changes in the ratio of hydrogenated to non-hydrogenated carbon bonds ($CC_{(1)}/CC_{(2)}$) compared to the reference value (see Table 2) suggest that the lapping process had a low influence on the termination bonds. Based on the SEM and AFM imaging and XPS analysis, it can be concluded that the BDD film did not crack due to CAML process.

Finally, Dynamic Electrochemical Impedance Spectroscopy (DEIS) study was performed under potentiodynamic conditions for deep anodic polarization of up to +2.5 V vs $Ag|Ag_2SO_4$, to cross-validate the nature of electrochemical modification of Si/BDD electrode via CAML. The experiment was carried out in 1 M H_2SO_4 and under conditions that imitate the author's previous study on the surface termination of boron-doped electrodes [36,44]. The cyclic voltammetry curve in anodic polarization range is presented in Fig. 7a, while Fig. 7b shows a typical 3D Nyquist plot versus anodic polarization scan, as obtained from the DEIS experiment.

The electric equivalent circuit chosen for electrochemical characterization of investigated system is shown in the inset of Fig. 7b. It is composed of high- and low- frequency time constants. The high-frequency time constant (C_1, R_1) is strongly correlated with the electrode contamination and termination type and typically fades away after the first polarization cycle [44,91]. Similar behavior occurs as a result of CAML pretreatment. The resistance of low frequency time constant is primarily associated with the charge transfer resistance R_{CT}. A constant phase element with the admittance $1/Z = Q_{CPE}(j\omega)^n$ is proposed in majority of studies dealing with BDD electrodes. Its origin is more complex. The dispersion of capacitance behavior is attributed to nonhomogeneous reaction rates along the areas of different boron-dopant concentration [6,87,95–98]. Furthermore, the resulting capacitance of a semiconductor surface is the sum of space-charge capacitance, the Helmholtz layer and the diffuse layer capacitance; the smallest of these three parameters will have the highest influence on the measured Q_{CPE}. In the presence of the excess of electrolyte, the diffuse layer capacitance can be neglected [74]. Space-charge capacitance dominates the value of Q_{CPE} at low overpotentials. However, at polarization potential exceeding +1.4 V

Table 2
Chemical composition of Si/BDD on the base of high-resolution XPS analysis in the energy range of C1s, O1s and Si2p3.

	BE/eV	t/min					
		0	3	10	30	80	120
$CC_{(1)}$	284.4	79.9	62.1	57.5	63.9	58.6	64.5
$CC_{(2)}$	285.0	16.6	14.9	11.4	11.9	14.3	11.9
$CO_{(1)}$	285.8	1.8	4.0	5.9	7.5	6.7	6.4
$CO_{(2)}$	286.8	–	2.8	6.2	2.4	3.3	2.4
$CO_{(3)}$	288.5	–	1.0	1.7	0.7	1.3	0.9
O	*	1.7	13.3	15.2	12.2	14.0	12.2
Si	103.6	–	1.9	2.1	1.4	1.8	1.7
CC/CO		53.6	9.9	5.0	7.2	6.5	7.9
$CC_{(1)}/CC_{(2)}$		4.8	4.2	5.0	5.4	4.1	5.4
O/Si		–	7.0	7.2	8.7	6.1	7.2

* The percentage composition of oxygen is a sum of three overlapping peaks, located at 531.1 eV, 532.0 eV and 533.1 eV. These derivate from C—O, C=O bonds and SiO2, respectively as well as other possible oxygen contaminations from pads.

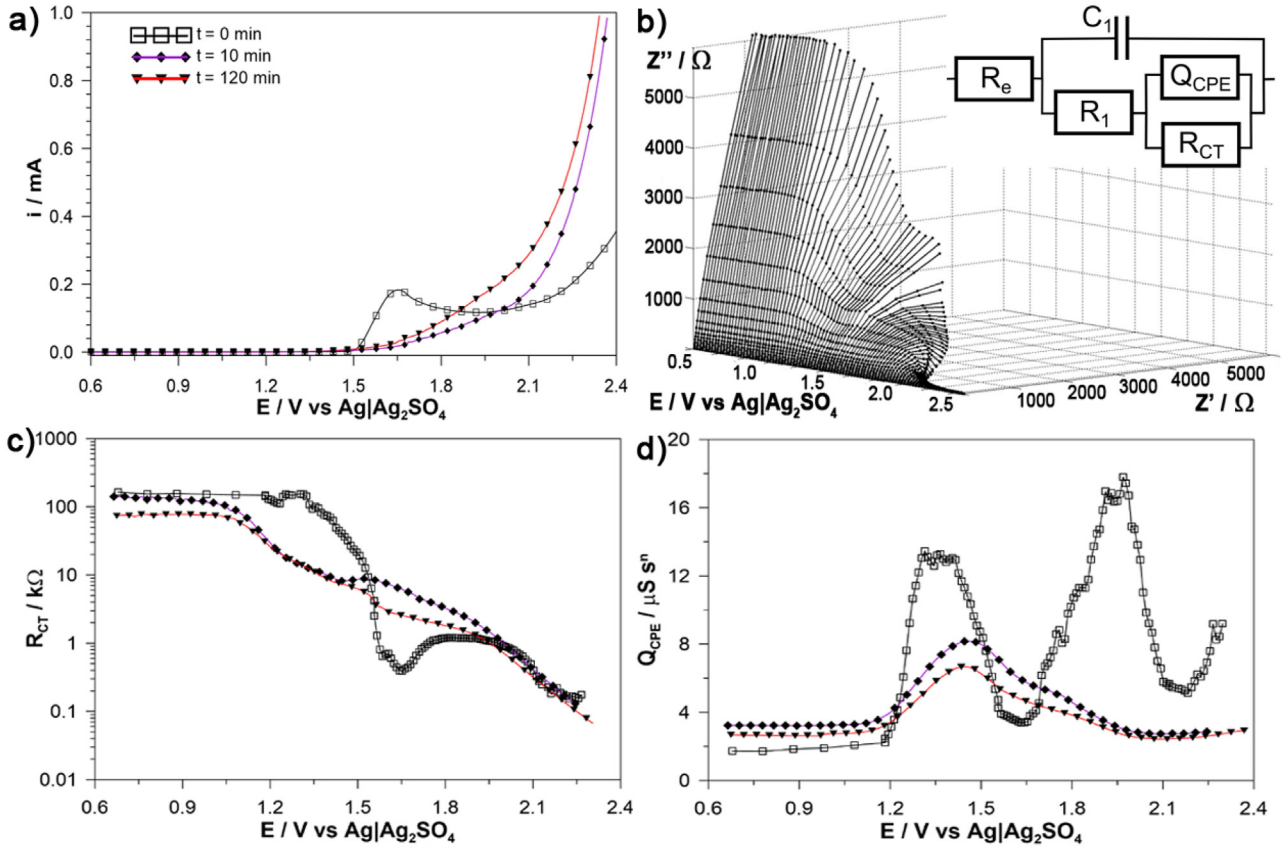

Fig. 7. a) Cyclic voltammetry in anodic polarization direction of Si/BDD electrode with superimposed DEIS signal after different CAML length b) 3D Nyquist plot vs anodic polarization depth for BDD sample at t = 120 min obtained from DEIS in potentiodynamic mode; c) R_{CT} and d) Q_{CPE} changes under anodic polarization, on the base of fitting procedure with equivalent circuit $R_e(C_1(R_1(Q_{CPE}R_{CT})))$.

vs $Ag|Ag_2SO_4$ electrochemical processes are involved resulting in significant contribution of double-layer capacitance. Here, the removal of sp^2-carbon contamination and subsequent functionalization of termination groups as well as water electrolysis should be considered. These findings should be considered even for metal-like BDD electrodes because of the limited density of charge carriers and heterogeneous behavior of individual grains [2,30].

Instantaneous values of low-frequency parameters, i.e. charge transfer resistance R_{CT} and constant phase element Q_{CPE} are plotted versus anodic polarization in Fig. 7c, d. The most interesting feature can be observed on Q=f(E) plot for the reference sample, in the form of peaks at approx. +1.4 and +2.0 V vs $Ag|Ag_2SO_4$. Such behavior is characteristic for relaxation processes [45] and might be connected with corrosion of sp^2-carbon contaminations from the electrode surface under anodic polarization [81,99–102].

Anodic polarization affects the presence of oxygen functional groups and removal of surface and subsurface hydrogen, influencing conduction and valence band positions and as a consequence space-charge capacitance through Mott-Schottky relationship [103–107]. The as-grown BDD is typically characterized by more steep $1/C_{sc}^2$ function than anodically treated electrode. This shift in behavior would decrease the value of Q_{CPE} during an on-line measurement [105–108].

The height as well as the area underneath above discussed peaks are much smaller after CAML pretreatment and they fade away with progressing duration of the process. Here, a peak in the function Q = f(E) located at +1.4 V vs $Ag|Ag_2SO_4$ is visible, arguably assisted by the second, smaller component, peaking at +1.7 V vs $Ag|Ag_2SO_4$. The peak at +2.0 V vs $Ag|Ag_2SO_4$ is missing.

The rapid disappearance of the second capacitive peak could be speculatively interpreted by different removal rates of grains with different crystallographic orientation. In their study, Pleskov et al. [86] revealed that (110) and (111)-oriented BDD grains possess more positive value of flat-band potential E_{fb} than (100)-oriented grains. The difference of +0.3 V for (110) and +0.6 V for (111)-oriented grains is in perfect agreement with the observed potential gap between the capacitance peaks, manifesting consecutive stages of the oxidation process. The disappearance of the capacitance peak at +2.0 V vs $Ag|Ag_2SO_4$ would in this case corroborate with (111)-oriented grains removal, as observed under SEM.

On the other hand, the DEIS measurements revealed the lack of a local minimum for the function $R_{CT} = f(E)$ at +1.6 V vs $Ag|Ag_2SO_4$, resulting from the absence of electrochemical corrosion of sp^2-carbon contaminations. An earlier and flatter decrease in this parameter's value with increasing anodic polarization was observed, which is in agreement with the findings about the lower energy requirement for the oxidation of termination bonds in the absence of non-diamond impurities [36,86]. For anodic polarization exceeding 2.0 V vs $Ag|Ag_2SO_4$, there was no observable difference in a slope of the function $R_{CT} = f(E)$ between the reference and CAML pretreated samples. After the oxidation of carbon contaminants on the electrode surface, this parameter became strongly influenced by the polarization resistance. Moreover, after a 120-min CAML, an almost four-fold decrease in R_{CT} at low anodic polarization was noted in comparison to the procedure without CAML. This points to the lowered charge transfer resistance due to lapping and thus is consistent with the

AFM results about the development of electrochemically-active surface.

4. Summary

The effect of chemical-assisted mechanical lapping of Si/BDD films by silica slurry was analyzed and discussed. A direct relationship between CAML and BDD performance was revealed at the macroscale. As a result of CAML process, the electric and electrochemical performance of the electrode has improved. This phenomenon should be mainly attributed to an increase in the surface fraction covered by the inter-grain regions, due to higher B dopant concentration, as well as the consecutive removal of amorphous-C, and *sp*- and sp^2-hybridized carbon.

As a consequence of CAML, the average grain size of crystallites decreased, which was followed by the gradual removal of (111) and (110)-oriented planes. Furthermore, altered oxidation kinetics of BDD electrodes was observed in association with the removal of the above-mentioned carbon impurities. The longer duration of CAML pretreatment had minor or detrimental effect on the BDD surface morphology and electrochemical performance. Based on the XPS analysis, the changes in surface chemistry of Si/BDD electrodes, due to a small amount of impurities introduced via silica slurry and pad, were revealed. These impurities had a negligible effect on electrochemical activity.

We demonstrated that short-duration CAML pretreatments should be applied to achieve efficient BDD surface activation, while, at the same time, CAML causes negligible alterations in the diamond film properties. The duration of pretreatment should be strictly controlled because the BDD surface defects, such as edge micro-chipping of crystallites and micro-cavities, were observed in the case of prolonged lapping.

In summary, CAML offers a possibility of a fast route towards increased electrochemical performance of highly-doped thin film electrodes, which may be used in numerous sensing applications. The process offers higher electrochemical activity at lower cost in comparison to hydrogen plasma pretreatment. CAML is less invasive than anodic electrochemical treatment or acid washing, which both affect termination type causing changes in the physico-chemical properties. Aforementioned techniques as well as cathodic electrochemical pre-treatment often lead to irreversible degradation of the BDD film, which is not the case for short CAML periods. Moreover, this unique pretreatment technique could also be applied to diamond-polymer composite electrodes in cases where plasma or acid pretreatments are destructive and thus not advised.

Acknowledgements

The authors gratefully acknowledge the financial support from the Polish National Science Centre (NCN) under grant no. 2015/17/D/ST5/02571 and 2014/14/M/ST5/00715. Authors are grateful to Michal Sobaszek, Department of Metrology and Optoelectronics of Gdansk University of Technology for preparation of Si/BDD samples.

Appendix A. Supplementary data

Supplementary data associated with this article can be found, in the online version, at http://dx.doi.org/10.1016/j.electacta.2017.05.027.

References

[1] L.A. Hutton, J.G. Iacobini, E. Bitziou, R.B. Channon, M.E. Newton, J.V. Macpherson, Examination of the Factors Affecting the Electrochemical Performance of Oxygen-terminated Polycrystalline Boron-doped Diamond Electrodes, Anal. Chem. 85 (2013) 7230–7240, doi:http://dx.doi.org/10.1021/ac401042t.

[2] H.V. Patten, K.E. Meadows, L.A. Hutton, J.G. Iacobini, D. Battistel, A.W. McKelvey, M.E. Newton, J.V. Macpherson, P.R. Unwin, Electrochemical Mapping Reveals Direct Correlation Between Heterogeneous Electron-transfer Kinetics and Local Density of States in Diamond Electrodes, Angew. Chemie. Intl. Ed. 51 (2012) 7002–7006, doi:http://dx.doi.org/10.1002/anie.201203057.

[3] I. Duo, A. Fujishima, C. Comninellis, Electron Transfer Kinetics on Composite Diamond (sp3)-graphite (sp2) Electrodes, Electrochem. Commun. 5 (2003) 695–700, doi:http://dx.doi.org/10.1016/S1388-2481(03)00169-3.

[4] G.M. Swain, The Susceptibility to Surface Corrosion in Acidic Fluoride Media: a Comparison of Diamond, HOPG and Glassy Carbon Electrodes, J. Electrochem. Soc. 141 (1994) 3382–3383, doi:http://dx.doi.org/10.1149/1.2059343.

[5] A. Zieliński, R. Bogdanowicz, J. Ryl, L. Burczyk, K. Darowicki, Local Impedance Imaging of Boron-doped Polycrystalline Diamond Thin Films, Appl. Phys. Lett. 105 (2014) 131908, doi:http://dx.doi.org/10.1063/1.4897346.

[6] S.C.B. Oliveira, A.M. Oliveira-Brett, Voltammetric and electrochemical impedance spectroscopy characterization of a cathodic and anodic pre-treated boron doped diamond electrode, Electrochim Acta 55 (2010) 4599–4605, doi:http://dx.doi.org/10.1016/j.electacta.2010.03.016.

[7] I. Duo, C. Levy-Clement, A. Fujishima, C. Comninellis, Electron Transfer Kinetics on Boron-doped diamond Part I: Influence of anodic treatment, J. Appl. Eletrochem. 34 (2004) 935–943, doi:http://dx.doi.org/10.1023/B:JACH.0000040525.76264.16.

[8] R. Ramesham, M.F. Rose, Polishing of Polycrystalline Diamond by Hot Nickel Surface, Thin Solid Films 320 (1998) 223–227, doi:http://dx.doi.org/10.1016/S0040-6090(97)00944-9.

[9] M.C. Granger, M. Witek, J. Xu, J. Wang, M. Hupert, A. Hanks, M.D. Koppang, J.E. Butler, G. Lucazeau, M. Mermoux, J.W. Strojek, G.M. Swain, Standard Electrochemical Behavior of High-Quality, Boron-Doped Polycrystalline Diamond Thin-Film Electrodes, Anal. Chem. 72 (2000) 3793–3804, doi:http://dx.doi.org/10.1021/ac0000675.

[10] Y. Jiang, D. Liu, Z. Jiang, B. Mao, X. Ma, Q. Li, Investigation on Electrochemically Cathodic Polarization of Boron-Doped Diamond Electrodes and Its Influence on Lead Ions Analysis, J. Electrochem. Soc. 161 (2014) H410–H415, doi:http://dx.doi.org/10.1149/2.106406jes.

[11] L.C.D. Santos, A.B. Couto, J.T. Matushima, M.R. Baldan, N.G. Ferreira, Anodic and Cathodic pre-Treatment effects on BDD surface to deposit copper nanoparticles applied to nitrate reduction, Mater. Res. S. C. 1395 (2012) 63–68, doi:http://dx.doi.org/10.1557/opl.2012.79.

[12] A.M. Ozkan, A.P. Malshe, W.D. Brown, Sequential Multiple-laser-assisted Polishing of Free-standing CVD Diamond Substrates, Diam. Relat. Mater. 6 (1997) 1789–1798, doi:http://dx.doi.org/10.1016/S0925-9635(97)00141-6.

[13] A. Hirata, H. Tokura, M. Yoshikawa, Smoothing of Chemically Vapour Deposited Diamond Films by Ion Beam Irradiation, Thin Solid Films 212 (1992) 43–48, doi:http://dx.doi.org/10.1016/0040-6090(92)90498-Z.

[14] A.M. Zaitsev, G. Kosaca, B. Richarz, V. Raiko, R. Job, T. Fries, W.R. Fahrner, Thermochemical Polishing of CVD Diamond Films, Diam. Relat. Mater. 7 (1998) 1108–1117, doi:http://dx.doi.org/10.1016/S0925-9635(98)00158-7.

[15] M. Panizza, G. Sine, I. Duo, L. Ouattara, C. Comninellis, Electrochemical Polishing of Boron-doped Diamond in Organic Media, Electrochem. Solid-State Lett. 6 (2003) D17–D19, doi:http://dx.doi.org/10.1149/1.161964.

[16] G.R. Salazar-Banda, A.E. de Carvalho, L.S. Andrare, R.C. Rocha-Filho, L.A. Avaca, On the Activation and Physical Degradation of Boron-Doped Diamond surfaces brought on by cathodic treatment, J. Appl. Electrochem. 40 (2010) 1817–1827, doi:http://dx.doi.org/10.1007/s10800-010-0139-1.

[17] A.P. Malshe, B.S. Park, W.D. Brown, H.A. Naseem, A Review of Techniques for Polishing and Planarizing Chemically Vapor-deposited (CVD) Diamond Films and Substrates, Diam. Relat. Mater. 8 (1999) 1198–1213, doi:http://dx.doi.org/10.1016/S0925-9635(99)00088-6.

[18] O.A. Williams, R.B. Jackman, Surface Conductivity on Hydrogen Terminated Diamond, Semicond. Sci. Technol. 18 (2003) S34–S40, doi:http://dx.doi.org/10.1088/0268-1242/18/3/305.

[19] T. Watanabe, Y. Honda, K. Kanda, Y. Einaga, Tailored design of boron-doped diamond electrodes for various electrochemical applications with boron-doping level and sp2-bonded carbon impurities, Phys. Status Solidi A 12 (2014) 2709–2717, doi:http://dx.doi.org/10.1002/pssa.201431455.

[20] N. Simon, H. Girard, D. Ballutaud, S. Ghodbane, A. Deneuville, M. Herlem, A. Etchberry, Effect of H and O Termination on the Charge Transfer of Moderately Boron Doped Diamond Electrodes, Diam. Relat. Mater. 14 (2005) 1179–1182, doi:http://dx.doi.org/10.1016/j.diamond.2004.12.013.

[21] S. Szunerits, R. Boukherroub, Different Strategies for Functionalization of Diamond Surface, J. Solid State Electrochem. 12 (2008) 1205–1218, doi:http://dx.doi.org/10.1007/s10008-007-0473-3.

[22] R. Bogdanowicz, M. Sawczak, P. Niedzialkowski, P. Zieba, B. Finke, J. Ryl, T. Ossowski, Direct Amination of Boron-doped Diamond by Plasma Polymerized Allylamine Film, Phys. Status Solidi. A 211 (2014) 2319–2327, doi:http://dx.doi.org/10.1002/pssa.201431242.

[23] C. Deslouis, J/De Sanoit, S. Saada, C. Mer, A. Pailleret, H. Cachet, P. Bergonzo, Electrochemical Behaviour of (111) B-doped Polycrystalline Diamond: Morphology/Surface conductivity/Activity Assessed by EIS and CS-AFM, Diam. Relat. Mater. 20 (2011) 1–10, doi:http://dx.doi.org/10.1016/j.diamond.2010.10.005.

[24] M. Tsigkourakos, T. Hantschel, D.K. Simon, T. Nuytten, A.S. Verhulst, B. Douhard, W. Vandervorst, On the Local Conductivity of Individual Diamond Seeds and Their Impact on the Interfacial Resistance of Boron-doped Diamond Films, Carbon 79 (2014) 103–112, doi:http://dx.doi.org/10.1016/j.carbon.2014.07.048.
[25] K.B. Holt, A.J. Bard, Y. Show, G.M. Swain, Scanning Electrochemical Microscopy and conductive Probe Atomic Force Microscopy Studies of Hydrogen-Terminated Boron-Doped Diamond Electrodes with Different Doping Levels, J. Phys. Chem. B 108 (2004) 15117–15127, doi:http://dx.doi.org/10.1021/jp048222x.
[26] D. Becker, K. Juttner, Influence of Surface Inhomogeneities of Boron Doped CVD-diamond electrodes on reversible charge transfer reactions, J. Appl. Electrochem. 33 (2003) 959–967, doi:http://dx.doi.org/10.1023/A:1025872013482.
[27] D. Becker, K. Juttner, The Impedance of Fast Charge Transfer reaction on Boron Doped Diamond Electrodes, Electrochim. Acta 49 (2003) 29–39, doi:http://dx.doi.org/10.1016/j.electacta.2003.04.003.
[28] T. Gueshi, K. Tokuda, H. Matsuda, Voltammetry at Partially Covered Electrodes: Part I. Chronopotentiometry and Chronoamperometry at Model Electrodes, J. Electroanal. Chem. 89 (1978) 247–260, doi:http://dx.doi.org/10.1016/S0022-0728(78)80188-0.
[29] T. Gueshi, K. Tokuda, H. Matsuda, Voltammetry at Partially Covered Electrodes: Part II. Linear potential sweep and cyclic voltammetry, J Electroanal, Chem. 101 (1979) 29–38, doi:http://dx.doi.org/10.1016/S0022-0728(79)80076-5.
[30] S. Szunerits, M. Mermoux, A. Crisci, B. Marcus, P. Bouvier, D. Delabouglise, J.P. Petit, S. Janel, R. Boukherroub, L. Tay, Raman Imaging and Kelvin Probe Microscopy for the Examination of the Heterogeneity of Doping in Polycrystalline Boron-Doped Diamond Electrodes, J. Phys. Chem. B 110 (2006) 23888–23897, doi:http://dx.doi.org/10.1021/jp064429.
[31] L.R. Radovic, Chemistry and Physics of Carbon, vol 29, CRC Press, New York, 2004.
[32] J. Perriere, E. Millon, E. Fogarassy, Recent Advances in Laser Processing of Materials, 1 st ed., Elsevier Science, New York, 2006.
[33] R. Bogdanowicz, M. Sobaszek, J. Ryl, M. Gnyba, M. Ficek, L. Golunski, W.J. Bock, M. Smietana, K. Darowicki, Improved Surface Coverage of an Optical Fibre with Nanocrystalline Diamond by the Application of Dip-coating Seeding, Diam. Relat. Mater. 55 (2015) 52–63, doi:http://dx.doi.org/10.1016/j.diamond.2015.03.007.
[34] E.L.H. Thomas, G.W. Nelson, S. Mandal, J.S. Foord, O.A. Williams, Chemical Mechanical Polishing of Thin Film Diamond, Carbon 68 (2014) 473–479, doi:http://dx.doi.org/10.1016/j.carbon.2013.11.023.
[35] P.B. Zantye, A. Kumar, A.K. Sikder, Chemical Mechanical Planarization for Microelectronics Application, Mater. Sci. Eng. R-Rep. 45 (2004) 89–220, doi:http://dx.doi.org/10.1016/j.mser.2004.06.002.
[36] J. Ryl, L. Burczyk, R. Bogdanowicz, M. Sobaszek, K. Darowicki, Study on Surface Termination of Boron-doped Diamond Electrodes under Anodic Polarization in H2SO4 by Means of Dynamic Impedance Technique, Carbon 96 (2016) 1093–1105, doi:http://dx.doi.org/10.1016/j.carbon.2015.10.064.
[37] M. Velicky, K.Y. Tam, R.A.W. Dryfe, On the Stability of the Silver/silver Sulfate Reference Electrode, Anal. Methods 4 (2012) 1207–1211, doi:http://dx.doi.org/10.1039/C2AY00011C.
[38] G.P. Morris, A.N. Simonov, E.A. Mashkina, R. Bordas, K. Gillow, R.E. Baker, D.J. Gavaghan, A.M. Bond, A Comparison of Fully Automated Methods of Data Analysis and Computer Assisted Heuristic Methods in an Electrode Kinetic Study of the Pathological Variable [Fe(CN)6]3-/4- Process by AC Voltammetry, Anal. Chem. 85 (2013) 11780–11787, doi:http://dx.doi.org/10.1021/ac4022105.
[39] A.N. Patel, M. Guille Collignon, M.A. O'Connell, W.O.Y. Hung, K. McKelvey, J.V. Macpherson, P.R. Unwin, A new View of Electrochemistry at Highly Oriented Pyrolytic Graphite, J. Am. Chem. Soc. 134 (2012) 20117–20130, doi:http://dx.doi.org/10.1021/ja308615h.
[40] P. Chen, R.L. McCreery, Control of Electron Transfer Kinetics at Glassy Carbon Electrodes by Specific Surface Modification, Anal. Chem. 68 (1996) 3958–3965, doi:http://dx.doi.org/10.1021/ac960492r.
[41] D. Necas, P. Klapetek, Gwyddion: an Open-source Software for SPM Data Analysis, Cent. Eur. J. Phys. 10 (2012) 181–188, doi:http://dx.doi.org/10.2478/s11534-011-0096-2.
[42] T. Trenkler, T. Hantschel, R. Stephenson, P. De Wolf, W. Vandervorst, Evaluating Probes for Electrical Atomic Force Microscopy, J. Vac. Sci. Technol. B. 18 (2000) 418–427, doi:http://dx.doi.org/10.1116/1.591205.
[43] A. Zieliński, K. Darowicki, Implementation and Validation of Multisinusoidal, Fast Impedance Measurements in Atomic Force Microscope Contact Mode, Microsc. Microanal. 20 (2014) 974–981, doi:http://dx.doi.org/10.1017/S1431927614000531.
[44] J. Ryl, R. Bogdanowicz, P. Slepski, M. Sobaszek, K. Darowicki, Dynamic Electrochemical Impedance Spectroscopy (DEIS) as a Tool for Analyzing Surface Oxidation Processes on Boron-doped Diamond Electrodes, J. Electrochem. Soc. 161 (2014) H359–H364, doi:http://dx.doi.org/10.1149/2.016406jes(/DOI.
[45 vitation Erosion under the Influence of Corrosive Factors, J. Electrochem. Soc. 155 (2008) P 44–P 49, doi:http://dx.doi.org/10.1149/1.2840619(/DOI.
[46] K. Darowicki, P. Slepski, Dynamic Electrochemical Impedance Spectroscopy of the First Order Electrode Reaction, J. Electroanal. Chem. 547 (2003) 1–8, doi:http://dx.doi.org/10.1016/S0022-0728(03)00154-2.
[47] A. Zielinski, Application of Different Modes of Nanoscale Impedance Microscopy in Materials Research, Surf. Innov. 3 (2015) 181–189, doi:http://dx.doi.org/10.1680/jsuin.15.00006.
[48] Z. Xu, T. Hantschel, M. Tsigkourakos, W. Vandervorst, Scanning Spreading Resistance Microscopy for Electrical Characterization of Diamond Interfacial Layers, Phys. Status Solidi A 212 (2015) 2578–2582, doi:http://dx.doi.org/10.1002/pssa.201532234.
[49] R. O'Hayre, M. Lee, F.B. Prinz, Ionic and electronic Impedance Imaging Using Atomic Force Microscopy, J. Appl. Phys. 95 (2004) 8382–8392, doi:http://dx.doi.org/10.1063/1.1737047.
[50] A. Arutunow, K. Darowicki, A. Zielinski, Atomic Force Microscopy Based Approach to Local Impedance Measurements of Grain Interiors and Grain Boundaries of Sensitized AISI 304 Stainless Steel, Electrochim. Acta 56 (2011) 2372–2377, doi:http://dx.doi.org/10.1016/j.electacta.2010.11.079.
[51] S.M. Gheno, R.H.G.A. Kiminami, M.M. Morelli, J.V. Bellini, P.I. Paulin Filhoz, An AFM/EFM Study of the Grain Boundary in ZnO-based Varistir Materials, J. Am. Ceram. Soc. 91 (2008) 3593–3598, doi:http://dx.doi.org/10.1111/j. 1551-2916.2008.02704.x.
[52] S. Wang, G.M. Swain, Spatially Heterogeneous Electrical and Electrochemical Properties of Hydrogen-Terminated Boron-Doped Nanocrystalline Diamond Thin Film Deposited from an Argon-Rich CH4/H2/Ar/B2H6 Source Gas Mixture, J. Phys. Chem. C 111 (2007) 3986–3995, doi:http://dx.doi.org/10.1021/jp0669557.
[53] S. Wang, V.M. Swope, J.E. Butler, T. Feygelson, G.M. Swain, The Structural and Electrochemical Properties of Boron-doped Nanocrystalline Diamond Thin-film Electrodes Grown from Ar-rich and H2-rich Source Gases, Diam. Relat. Mater. 18 (2009) 669–677, doi:http://dx.doi.org/10.1016/j.diamond.2008.11.033.
[54] B.L. Willems, G. Zhang, J. Vanacken, V.V. Moshchalkov, S.D. Janssens, K. Haenen, P. Wagner, Granular Superconductivity in Metallic and Insulating Nanocrystalline Boron-Doped Diamond Thin Films, J Phys. D 43 (2010) 37409, doi:http://dx.doi.org/10.1088/0022-3727/43/37/374019.
[55] Z. Vlckova Zivcova, O. Frank, V. Petrak, H. Tarabkova, J. Vacık, M. Nesladek, L. Kavan, Electrochemistry and in Situ Raman Spectroelectrochemistry of Low and High Quality Boron Doped Diamond Layers in Aqueous Electrolyte Solution, Electrochim. Acta 87 (2013) 518–525, doi:http://dx.doi.org/10.1016/j.electacta.2012.09.031.
[56] Y.G. Lu, S. Turner, J. Verbeeck, S.D. Janssens, P. Wagner, K. Haenen, G. Van Tendeloo, Direct Visualization of Boron Dopant Distribution and Coordination in Individual Chemical Vapor Deposition Nanocrystalline B-doped Diamond Grains, Appl. Phys. Lett. 101 (2012) 041907, doi:http://dx.doi.org/10.1063/1.4738885.
[57] P. Ashcheulov, J. Sereba, A. Kovalenko, V. Petrak, F. Fendrych, M. Nesladek, A. Taylor, Z. Vlckova Zivcova, O. Frank, L. Kavan, M. Dracinsky, P. Hubik, J. Vacik, I. Kraus, I. Kratochvilova, Conductivity of Boron-Doped Polycrystalline Diamond Films: Influence of Specific Boron Defects, Eur. Phys. J. B 86 (2013) 443, doi:http://dx.doi.org/10.1140/epjb/e2013-40528-x.
[58] K.E. Bennet, K.H. Lee, J.N. Kruchowski, S.Y. Chang, M.P. Marsh, A.A. Van Orsow, A. Paez, F.S. Manciu, Development of Conductive Boron-Doped Diamond Electrode: A microscopic, Spectroscopic, and Voltammetric Study, Materials 6 (2013) 5726–5741, doi:http://dx.doi.org/10.3390/ma6125726.
[59] G. Zhang, S. Turner, E.A. Ekimov, J. Vanacken, M. Timmermans, T. Samuely, V. A. Sidorov, S.M. Stishov, Y. Lu, B. Deloof, B. Goderis, G.V. Tendeloo, J. Van de Vondel, V.V. Moshchalkov, Global and Local Superconductivity in Boron-Doped Granular Diamond, Adv. Mater. 26 (2014) 2034–2040, doi:http://dx.doi.org/10.1002/adma.201304667.
[60] J. Chevallier, B. Theys, A. Lusson, C. Grattepain, A. Deneuville, E. Gheeraert, Hydrogen-boron Interactions in p-type Diamond, Phys. Rev. B. 58 (1998) 7966–7969, doi:http://dx.doi.org/10.1103/PhysRevB.58.7966.
[61] J. Chevallier, A. Lusson, D. Ballutaud, B. Theys, F. Jomard, A. Deneuville, M. Bernard, E. Gheeraert, E. Bustarret, Hydrogen-acceptor Interactions in Diamond, Diam. Relat. Mater. 10 (2001) 399–404, doi:http://dx.doi.org/10.1016/S0925-9635(00)00432-5.
[62] K.M. Rutledge, K.K. Gleason, Hydrogen in CVD Diamond Films, Chem. Vap. Depos. 2 (1996) 37–43, doi:http://dx.doi.org/10.1002/cvde.19960020203.
[63] Y. Show, M.A. Witek, P. Sonthalia, G.M. Swain, Characterization and Electrochemical Responsiveness of Boron-doped Nanocrystalline Diamond Thin-film Electrodes, Chem. Mater. 15 (2003) 879–888, doi:http://dx.doi.org/10.1021/cm020927t.
[64] N.R. Wilson, S.L. Clewes, M.E. Newton, P.R. Unwin, J.V. Macpherson, Impact of Grain-dependent Boron Uptake on the Electrochemical and Electrical Properties of Polycrystalline Boron Doped Diamond Electrodes, J. Phys. Chem. B 110 (2006) 5639–5646, doi:http://dx.doi.org/10.1021/jp0547616.
[65] G.M. Swain, R. Ramesham, The Electrochemical Activity of Boron-Doped Polycrystalline Diamond Thin Film Electrodes, Anal. Chem. 65 (1993) 345–351, doi:http://dx.doi.org/10.1021/ac00052a007.
[66] K. Cinkova, C. Batchelor-McAuley, M. Marton, M. Vojs, L. Svorc, R.G. Compton, The Activity of Non-Metallic Boron-Doped Diamond Electrodes with Sub-micron Scale Heterogeneity and the Role of the Morphology of sp2 Impurities, Carbon 110 (2016) 148–154, doi:http://dx.doi.org/10.1016/j.carbon.2016.09.015.
[67] N. Yang, J.S. Foord, X. Jiang, Diamond electrochemistry at the nanoscale: A review, Carbon 99 (2016) 90–110, doi:http://dx.doi.org/10.1016/j.carbon.2015.11.061.

[68] P. Delahay, Theory of Irreversible Waves in Oscillographic Polarography, J. Am. Chem. Soc. 75 (1953) 1190–1196, doi:http://dx.doi.org/10.1021/ja01101a054.
[69] S.J. Konopka, B. McDuffie, Diffusion Coefficients of Ferri- and Ferrocyanide Ions in Aqueous Media, Using Twin-electrode Thin-layer Electrochemistry, Anal. Chem. 42 (1970) 1741–1746, doi:http://dx.doi.org/10.1021/ac50160a042.
[70] T.J. Davies, C.E. Banks, R.G. Compton, Voltammetry at Spatially Heterogeneous Electrodes, J. Solid State Electrochem. 9 (2005) 797–808, doi:http://dx.doi.org/10.1007/s10008-005-0699-x.
[71] P. Rama Kant, Theory of Staircase Voltammetry and Linear Scan Voltammetry on Fractal Electrodes: Emergence of Anomalous Randles-Sevcik Behavior, Electrochim. Acta 111 (2013) 223–233, doi:http://dx.doi.org/10.1016/j.electacta.2013.07.163.
[72] L. Nyikos, T. Pajkossy, Diffusion to Fractal Surfaces, Electrochim. Acta 31 (1986) 1347–1350, doi:http://dx.doi.org/10.1016/0013-4686(86)80160-8.
[73] K. Jüttner, D. Becker, Characterization of Boron-Doped Diamond Electrodes by Electrochemical Impedance Spectroscopy, J. Appl. Electrochem. 37 (2006) 27–32, doi:http://dx.doi.org/10.1007/s10800-006-9228-6.
[74] M.H.P. Santana, L.A. De Faria, J.F.C. Boodts, Electrochemical Characterization and Oxygen Evolution at a Heavily Boron Doped Diamond Electrode, Electrochim. Acta 50 (2005) 2017–2027, doi:http://dx.doi.org/10.1016/j.electacta.2004.08.050.
[75] J.V. Macpherson, The Use of Conducting Diamond in Electrochemistry, in: R.C. Alkire, P.N. Bartlett Lipkowski (Eds.), Electrochemistry of Carbon Electrodes, J. Wiley, New York, 2016, pp. 163–210, doi:http://dx.doi.org/10.1002/9783527697489.ch5.
[76] T. Spataru, L. Preda, C. Munteanu, A.I. Caciuleanu, N. Spataru, A. Fujishima, Influence of Boron-Doped Diamond Surface Termination on the Characteristics of Titanium Dioxide Anodically Deposited in the Presence of a Surfactant, J. Electrochem. Soc. 162 (2015) H535–H540, doi:http://dx.doi.org/10.1149/2.0741508jes.
[77] C. Liao, Y. Wang, S. Yang, Depth Profiles of Boron and Hydrogen in Boron-doped diamond films and related performance characteristics, Diam. Relat. Mater. 8 (1999) 1229–1233, doi:http://dx.doi.org/10.1016/S0925-9635(99)00127-2.
[78] M. Tsigkourakos, T. Hantschel, Z. Xu, B. Douhard, J. Meersschaut, Y. Zou, K. Larsson, M. Boman, W. Vandervorst, Suppression of Boron Incorporation at the Early Growth Phases of Boron-doped Diamond Thin Films, Phys. Status Solidi A. 212 (2015) 2595–2599, doi:http://dx.doi.org/10.1002/pssa.201532185.
[79] S. Wang, Structure-Function Relationship of Boron-doped Diamond Thin-film Electrodes and Application for in Vitro Amperometric Measurements, Doctoral Dissertation, (2008) .
[80] R. Bogdanowicz, J. Czupryniak, M. Gnyba, J. Ryl, T. Ossowski, M. Sobaszek, E. M. Siedlecka, K. Darowicki, Amperometric Sensing of Chemical Oxygen Demand at Glassy Carbon and Silicon Eectrodes Modified with Boron-doped Diamond, Sensor. Actuat. B-Chem. 189 (2013) 30–36, doi:http://dx.doi.org/10.1016/j.snb.2012.12.007.
[81] J.V. Macpherson, A Practical Guide to Using Boron Doped Diamond in Electrochemical Research, Phys. Chem. Chem. Phys. 17 (2015) 2935–2949, doi:http://dx.doi.org/10.1039/C4CP04022H.
[82] Z.L. Wang, C. Lu, J.J. Li, C.Z. Gu, Effect of Gas Composition on the Growth and Electrical Properties of Boron-doped Diamond Films, Diam. Relat. Mater. 18 (2009) 132–135, doi:http://dx.doi.org/10.1016/j.diamond.2008.10.040.
[83] L. Pastewka, S. Moser, P. Gumbsch, M. Moseler, Anisotropic Mechanical Amorphization Drives Wear in Diamond, Nature Mater. 10 (2011) 34–38, doi:http://dx.doi.org/10.1038/NMAT2902.
[84] T. Schuelke, T.A. Grotjohn, Diamond Polishing, Diam. Relat. Mater. 32 (2013) 17–26, doi:http://dx.doi.org/10.1016/j.diamond.2012.11.007.
[85] E.M. Wilks, J. Wilks, The Resistance of Diamond to Abrasion, J. Phys. D: Appl. Phys. 5 (1972) 1902–1919, doi:http://dx.doi.org/10.1088/0022-3727/5/10/323(/DOI.
[86] Y.V. Pleskov, Y.U. Evstefeeva, V.P. Varnin, I.G. Teremetskaya, Synthetic Semiconductor Diamond Electrodes: Electrochemical Characteristics of Homoepitaxial Boron-doped Films Grown at the (111), (110), and (100) Faces of Diamond Crystals, Russ. J. Electrochem. 40 (2004) 886–892, doi:http://dx.doi.org/10.1023/B:RUEL.0000041354.70107.
[87] T. Kondo, K. Honda, D.A. Tryk, A. Fujishima, AC Impedance Studies of Anodically Treated Polycrystalline Homoepitaxial Boron-doped Diamond Electrodes, Electrochim Acta 48 (2003) 2739–2748, doi:http://dx.doi.org/10.1016/S0013-4686(03)00391-8.
[88] B.S. El-Dasher, J.J. Gray, J.W. Tringe, J. Biener, A.V. Hamza, C. Wild, E. Worner, P. Koidl, Crystallographic Anisotropy of Wear on a Polycrystalline Diamond Surface, Appl. Phys. Lett. 88 (2006) 241915, doi:http://dx.doi.org/10.1063/1.2213180.
[89] J. Zavazalova, K. Prochazkova, K. Schwarzova-Peckova, Boron-doped Diamond Electrodes for Voltammetric Determination of Benxophenone-3, Anal. Lett. 49 (2016) 80–91, doi:http://dx.doi.org/10.1080/00032719.2014.1003425.
[90] D. Ballutaud, N. Simon, H. Girard, E. Rzepka, B. Bouchet-Fabre, Photoelectron Spectroscopy of Hydrogen at the Polycrystalline Diamond Surface, Diam. Relat. Mater. 15 (2005) 716–719, doi:http://dx.doi.org/10.1016/j.diamond.2006.01.004.
[91] A. Denisenko, C. Pietzka, A. Romanyuk, H. El-Hajj, E. Kohn, The Electronic Surface Barrier of Boron-doped Diamond by Anodic Oxidation, J. Appl. Phys. 103 (2008) 014904, doi:http://dx.doi.org/10.1063/1.2827481.
[92] M. Wang, N. Simon, G. Charrier, M. Bouttemy, A. Etcheberry, M. Li, R. Boukherroub, S. Szunerits, Distinction Between Surface Hydroxyl and Ether Groups on Boron-doped Diamond Electrodes Using a Chemical Approach, Electrochem. Commun. 12 (2010) 351–354, doi:http://dx.doi.org/10.1016/j.elecom.2009.12.029.
[93] P. Niedzialkowski, R. Bogdanowicz, P. Zieba, J. Wysocka, J. Ryl, M. Sobaszek, T. Ossowski, Melamine-Modified Boron-Doped Diamond towards Enhanced Detection of Adenine, Guanine and Caffeine, Electroanal. 28 (2016) 211–221, doi:http://dx.doi.org/10.1002/elan.201500528.
[94] H. Girard, N. Simon, D. Ballutaud, A. Etcheberry, Correlation Between Flat-band Potential Position and Oxygenated Termination Nature on Boron-doped Diamond Electrodes, Comptes Rendus Chimie. 11 (2008) 1010–1015, doi:http://dx.doi.org/10.1016/j.crci.2008.01.014.
[95] B. Hirschorn, B. M.E.Orazem, V. Tribollet, I.Frateur Vivier, M. Musiani, Determination of Effective Capacitance and Film Thickness from Constant-Phase-Element Parameters, Electrochim. Acta 55 (2010) 6218–6227, doi:http://dx.doi.org/10.1016/j.electacta.2009.10.065.
[96] J. Hernando, S.Q. Lud, P. Bruno, D.M. Gruen, M. Stutzmann, J.A. Garrido, Electrochemical Impedance Spectroscopy of Oxidized and Hydrogen-Terminated Nitrogen-Induced Conductive Ultrananocrystalline Diamond, Electrochim. Acta 54 (2009) 1909–1915, doi:http://dx.doi.org/10.1016/j.electacta.2008.10.041.
[97] Y.V. Pleskov, M.D. Krotova, V.G. Ralchenko, A.V. Khomich, R.A. Khmelnitskiy, Vaccum-Annealed Undoped Polycrystalline CVD Diamond: a new Electrode Material, Electrochim. Acta 49 (2003) 41–49, doi:http://dx.doi.org/10.1016/j.electacta.2003.05.005.
[98] R. Trouillon, D. O'Hare, Comparison of Glassy Carbon and Boron Doped Diamond Electrodes: Resistance to Biofouling, Electrochim. Acta 55 (2010) 6586–6595, doi:http://dx.doi.org/10.1016/j.electacta.2010.06.016.
[99] B.P. Chaplin, D.K. Hubler, J. Farrell, Understanding Anodic Wear at Boron Doped Diamond Film Electrodes, Electrochim. Acta 89 (2013) 122–131, doi:http://dx.doi.org/10.1016/j.electacta.2012.10.166.
[100] T. Kashiwada, T. Watanabe, Y. Ootani, Y. Tateyama, Y. Einaga, A Study on Electrolytic Corrosion of Boron-doped Diamond Electrodes when Decomposing Organic Compounds, ACS Appl Mater. Interfaces 8 (2016) 28299–28305, doi:http://dx.doi.org/10.1021/acsami.5b11638.
[101] S. Garcia-Segura, E.V. Dos Santos, C.A. Martínez-Huitle, Role of sp3/sp2 Ratio on the Electrocatalytic Properties of Boron-doped Diamond Electrodes: A Mini Review, Electrochem. Commun. 59 (2015) 52–55, doi:http://dx.doi.org/10.1016/j.elecom.2015.07.002.
[102] Y. Einaga, J.S. Foord, G.M. Swain, Diamond Electrodes: Diversity and Maturity, Mater. Res. Bull. 39 (2014) 525–532, doi:http://dx.doi.org/10.1557/mrs.2014.94.
[103] P. Actis, A. Denoyelle, R. Boukherroub, S. Szunerits, Influence of the Surface Termination on the Electrochemical Properties of Boron-Doped Diamond (BDD) Interfaces, Electrochem. Comm. 10 (2008) 402–4063, doi:http://dx.doi.org/10.1016/j.elecom.2007.12.032.
[104] A.F. Azevedo, M.R. Baldin, N.G. Ferreira, Doping Level Influence on Chemical Surface of Diamond Electrodes, J. Phys. Chem. Solids 74 (2013) 599–604, doi:http://dx.doi.org/10.1016/j.jpcs.2012.12.013.
[105] H.B. Suffredini, V.A. Pedrosa, L. Codognoto, S.A.S. Machado, R.C. Rocha-Filho, L.A. Avaca, Enhanced Electrochemical Response of Boron-Doped Diamond Electrodes Brought on by a Cathodic Surface Pre-Treatment, Electrochem. Acta 49 (2004) 4021–4026, doi:http://dx.doi.org/10.1016/j.electacta.2004.01.082.
[106] H. Girard, N. Simon, D. Ballutaud, M. Herlem, A. Etcheberry, Effect of Anodic and Cathodic Treatments on the Charge Transfer of Boron Doped Diamond Electrodes, Diam. Rel. Mater. 16 (2007) 316–325, doi:http://dx.doi.org/10.1016/j.diamond.2006.06.009.
[107] T.N. Rao, D.A. Tryk, K. Hashimoto, A. Fujishima, Band-Edge Movements of Semiconducting Diamond in Aqueous Electrolyte Induced by Anodic Surface Treatment, J. Electrochem. Soc. 146 (1999) 680–684, doi:http://dx.doi.org/10.1149/1.1391662.
[108] N. Simon, H. Girard, M. Manesse, D. Ballutaud, A. Etcheberry, Electrochemical Preconditioning of Moderately Boron Doped Diamond Electrodes: Effect of annealing, Diam. Relat. Mater. 17 (2008) 1371–1375, doi:http://dx.doi.org/10.1016/j.diamond.2008.03.003.